applied sciences

MDPI

Article

Parameter Optimisation in Selective Laser Melting on C300 Steel

I. I. Cuesta [1,*], A. Díaz [1], M. A. Rojo [1], L. B. Peral [1,2], J. Martínez [3] and J. M. Alegre [1]

[1] Structural Integrity Group, Universidad de Burgos, Escuela Politécnica Superior, Avda. Cantabria s/n, 09006 Burgos, Spain
[2] Departamento de Ciencia de los Materiales e Ingeniería Metalúrgica, Escuela Politécnica de Ingenería de Gijón, University of Oviedo, Campus de Viesques, 33203 Gijón, Spain
[3] Samylabs, C/Astintze 6A, Oficina 001, 48160 Derio, Bizkaia, Spain
* Correspondence: iicuesta@ubu.es

Abstract: Additive manufacturing (AM) of metallic materials is increasingly being adopted in numerous sectors, such as biomedicine, aerospace or automotive industries, due to its versatility in the creation of complex geometries and the minimisation of material waste when compared to traditional subtractive methods. In order to ensure a reliable operation of these parts, however, an in-depth study of the effect of additive manufacturing on mechanical properties, including tensile, fatigue and fracture resistance, is necessary. Among the vast number of methods and materials, this project is focused in one of the most promising techniques for the industry: Selective Laser Melting (SLM) for the production of a tools steel, in particular C300 steel components for the automotive sector. The main objective of this paper is to optimise some of the key parameters in the printing process, such as laser power, laser speed and hatch spacing. These variables are essential to obtain parts with good resistance. To that purpose, tensile tests were performed in 3D printed specimens, and then elastoplastic properties were extracted, organised and analysed through a design of experiments for the subsequent output fitting using the response surface methodology.

Keywords: response surface; additive manufacturing; selective laser melting; C300 maraging steel

Citation: Cuesta, I.I.; Díaz, A.; Rojo, M.A.; Peral, L.B.; Martínez, J.; Alegre, J.M. Parameter Optimisation in Selective Laser Melting on C300 Steel. *Appl. Sci.* **2022**, *12*, 9786. https://doi.org/10.3390/app12199786

Academic Editors: Munish Kumar Gupta and Alberto José García Collado

Received: 16 August 2022
Accepted: 26 September 2022
Published: 28 September 2022

1. Introduction

Nowadays, the most widespread method for producing critical or high value parts from powder material is Additive Manufacturing. One of the most widely used techniques is Selective Laser Melting (SLM) due to its suitability for the production of prototypes and medium-sized parts, but also for the increasing capacity for manufacturing short runs. In addition, the range of metal alloys available in powder form is extensive, and the final component shows good properties, equivalent to those of traditional manufacturing processes [1–9].

SLM technology is based on the creation of a part by melting the material layer by layer using a high-power laser as a source of thermal energy. The laser beam is focused with a system of mirrors on a powder bed and follows layer by layer, while the layer thickness is controlled, the geometry having been previously designed within a CAD software. The powder receives the laser energy, melts and, once it solidified during subsequent cooling, is welded to the material forming the layer immediately below, thus ensuring good adhesion between layers.

This technology enables the production of complex three-dimensional parts with high precision (0.1 mm in 25 mm) and high surface finish quality (5–15 µm). Using the SLM technique it is possible to produce parts with values of up to 97–99% relative density. Therefore, this process can be used for the production of functional components and it is economically viable. In addition, recent advances in laser technology have extended and

generalised the process to different metallic materials, such as copper alloys, aluminium and tungsten [10].

The microstructure generated in the material has an intrinsic characteristic morphology, as a consequence of the superposition of successive molten layers of a few tens of micrometres, including the likely presence of defects or pores mainly at the melting edges. An interesting review of the mechanisms for defect formation in materials manufactured by SLM can be found in the work of Zhang et al. [11].

In this sense, it is necessary to study in depth the printing parameters to obtain materials with a microstructure that gives them good properties, similar to those that can be obtained with other conventional manufacturing methods. Especially in those materials that are newly considered for Additive Manufacturing, such as C300 steel, commonly used in mould tooling in the automotive sector.

The printing parameters are numerous, but three critical variables can be highlighted: laser power, laser speed and hatch spacing. These are the parameters studied in this research, representing the base of the considered design of experiments and the corresponding response surfaces. Design of experiments is a statistical technique to identify and quantify the most important factors in an experimental study. It has been used successfully in many fields since the early 1920s [12–15]. This technique facilitates the optimisation of the number of experiments performed to determine the influence of some input variables on the experimental outcome. This design is very important when tests are costly, either in a computational or economic sense, as well for minimising the duration of experimental campaigns.

For these reasons, the main objective of this paper is to optimise some of the key parameters in this process, such as laser power, laser speed and hatch spacing. These variables are essential for the production of parts with good resistance. In order to do this, tensile tests were performed in 3D printed specimens, and then elastoplastic properties were extracted, organised and analysed using design of experiments based on the response surface methodology.

2. Materials

The alloy selected for this research is a C300 steel alloy, classified as maraging steel. This steel has also other designations, such as 1.2709, M300 and tool steel. It is a low-carbon alloy with high nickel and cobalt contents. It has a superior mechanical strength due to intermetallic precipitates formed microscopically during the ageing treatment, such as Ni_3Ti and Fe_2Mo [16]. These compounds result in a higher hardness than conventional low-carbon martensitic steels. In addition, it has a high corrosion resistance, even at high temperatures up to 500 °C. For this reason this steel is used as tool steel, in moulding dies, missiles, rockets, engine casings and gears. Table 1 shows the composition of the C300 steel provided by the powder manufacturer (Oerlikon). In addition, the expected mechanical properties are also provided as a function of the printing orientation. For the vertical direction (Z) the expected yield strength ($\sigma_{0.2}$) is between 900 and 1100 MPa, the ultimate stress (σ_{uts}) between 1000 and 1200 MPa and the elongation (ε_r) between 6% and 14% without any ageing heat treatment. Taking these values into account, the area under the stress–strain curve (A) is expected to be between 60 and 170 MPa.

Table 1. Composition of C300 steel in weight percent (nominal).

Alloy	Ni	Mo	Co	Ti	C	Fe
C300	18	5.0	9.0	0.9	<0.03	Balance

This steel has just recently started to be used for Additive Manufacturing processes, where the presence of temperature gradients and the rapid solidification leads to a more heterogeneous structure, resulting in better mechanical properties in terms of strength and hardness. However, this also leads to the appearance of cracks, and it is hence necessary

to relieve residual stresses by means of heat treatments [17]. The specimens used in this research have not received the ageing heat treatment before testing. The metal powders used have been atomized with argon gas, are spheroidal in morphology and particles have an average size of 45 ± 15 µm.

3. Experimental Methodology

The SLM technology printer used was the ALBA 300 model developed jointly by the companies Samylabs and ONA. The machine has a CW fibre laser of 300 W, a wavelength of 1080 nm and a cylindrical working volume with a diameter of 160 mm and a height of 200 mm. It operates in a protected argon atmosphere to minimise oxygen uptake during printing. In addition, it is equipped with an oxygen sensor that monitors the chamber conditions in real time and ensures that the printing process cannot start until the oxygen-free conditions are met.

The main printing parameters—laser speed, laser hatching distance, layer height, wavelength and laser power—have a decisive influence on mechanical properties of the manufactured part, particularly on the values of yield strength ($\sigma_{0.2}$), ultimate stress (σ_{uts}), elongation (ε_r) and area under the stress–strain curve (A). This last parameter represents the total mechanical energy per unit volume absorbed by the material. These parameters, as mentioned above, must be optimised for each material, since the thermal properties and the laser radiation absorption of a certain wavelength result on different energy densities required for fusion.

In order to find these optimal parameters for C300 steel, a design of experiments using a response surface methodology has been established. Because of the difficulty of covering all these parameters in the response surface, it was decided to fix some of them. Thus, the wavelength, corresponding to the laser of the ALBA 300 printer, and the layer height have been fixed at 1080 nm and 40 µm, respectively. Therefore, the response surface of the four studied outcome variables ($\sigma_{0.2}$, σ_{uts}, ε_r and A) are determined by the parameters P, S and H. The range of variation of these parameters is shown in Table 2, where the values shown correspond to the interval [–1, 1] in the design of experiments.

Table 2. Parameters used in the design of experiments.

Variable Parameters	
Laser Power (P)	[200, 250] W
Scanning Speed (S)	[500–800] mm/s
Hatching Distance (H)	[0.08–0.14] mm

The relationship that exists among these three parameters and the values of the response surfaces can be expressed as $S = f(P^*, S^*, H^*)$, where f is postulated as a quadratic model, as expressed in Equation (1), in which P^*, S^* and H^* are the coded variables for P, S and H, respectively. The real parameter values are coded so all vary within the same interval, normalising the inputs and facilitating a precise estimation of the coefficients that define the function $f(P^*, S^*, H^*)$. For any real value X_i of the input parameters, coding can be performed through the Expression (2), resulting in the corresponding coded value x_i, where X_{iNInf} is the real value of the lowest level for the parameter i, X_{iNSup} is the real value of the highest level of the parameter i and $\widetilde{X}_i$ is the mean of the real values of the highest and lowest levels of the parameter i.

$$f(P^*, S^*, H^*) = b_0 + b_1 \cdot P^* + b_2 \cdot S^* + b_3 \cdot H^* + b_{11} \cdot P^{*2} + b_{22} \cdot S^{*2} + b_{33} \cdot H^{*2} + \\ + b_{12} \cdot P^* \cdot S^* + b_{13} \cdot P^* \cdot H^* + b_{23} \cdot S^* \cdot H^* \quad (1)$$

$$x_i = \frac{2 \cdot \left(X_i - \widetilde{X}_i \right)}{X_{iNSup} - X_{iNInf}} \qquad i = P^*, S^*, H^* \quad (2)$$

Coefficients of the function $f(P^*, S^*, H^*)$ for each material property outcome ($\sigma_{0.2}$, σ_{uts}, ε_r and A) are determined by performing a central cubic design experiment [18–20] using Design Expert software to estimate these coefficients. The main features of this design are:

- The use of three factors, namely, the parameters P^*, S^* and H^*.
- The choice of a cubic domain.
- The coding of the interval values for the three parameters listed in Table 2 using Expression (2).
- The cubic experiment matrix with three levels for each input parameter with two repetitions at the domain midpoint, in order to capture the variability of the test (experiment NUM. 15 and 16).
- The use of Expression (1) to fit the four response surfaces for the corresponding outcome properties.

Table 3 shows both the experiment matrix with the coded variables and with the actual testing values proposed for determining the coefficients of the function $f(P^*, S^*, H^*)$. Since all material properties ($\sigma_{0.2}$, σ_{uts}, ε_r and A) correspond to the same range of values for parameters P, S and H, the values in this table are valid for all cases.

Table 3. Proposed design of experiments.

Experiment	Experiment Matrix			Experimentation Plan		
NUM	**Power**	**Speed**	**Hatching**	**Power (W)**	**Speed (mm/s)**	**Hatching (mm)**
1	−1	−1	−1	200	500	0.08
2	1	−1	−1	250	500	0.08
3	−1	1	−1	200	800	0.08
4	1	1	−1	250	800	0.08
5	−1	−1	1	200	500	0.14
6	1	−1	1	250	500	0.14
7	−1	1	1	200	800	0.14
8	1	1	1	250	800	0.14
9	−1	0	0	200	650	0.11
10	1	0	0	250	650	0.11
11	0	−1	0	225	500	0.11
12	0	1	0	225	800	0.11
13	0	0	−1	225	650	0.08
14	0	0	1	225	650	0.14
15	0	0	0	225	650	0.11
16	0	0	0	225	650	0.11

4. Result and Discussion

To carry out this experimental plan, a round tensile specimen (4 mm of diameter) was printed for each of the matrix point; these conditions were subsequently tested in accordance with the ASTM E8M standard [21]. The printer software allows all the specimens to be manufactured together, assigning their corresponding parameters (P, S and H) to each one of them. Figure 1 shows the newly manufactured tensile specimens, as well as their final appearance (SLM condition without finishing treatment) before testing.

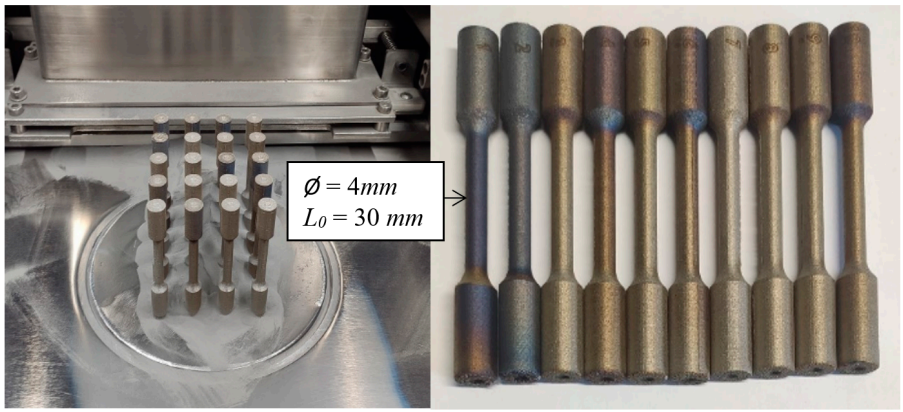

Figure 1. Tensile specimens manufactured using SLM.

After the test of each specimen, force–displacement data are processed in order to obtain the mechanical behaviour of each parameter combination. In this sense, Figure 2 shows some of the typical stress–strain curves obtained. Two types of behaviour can be clearly differentiated: one more brittle (specimens 7 and 8) and the other more ductile (specimens 1 and 15) where necking occurs in the specimen. In order to better compare this different behaviour, Figures 3 and 4 show the optical micrographs of all the specimens tested. The degree of ductility in each of them is directly related to the reduction in area that occurs in the failure zone. SEM micrographs have also been carried out. Figures 5 and 6 show those of specimens 1 and 15 with a ductile behaviour, dominated by the growth and coalescence of microvoids. In contrast, Figures 7 and 8 show the brittle behaviour of specimens 7 and 8. In the latter, it can be seen that the laser beam has not had enough energy to completely melt the net area of the specimen, which causes brittle failure.

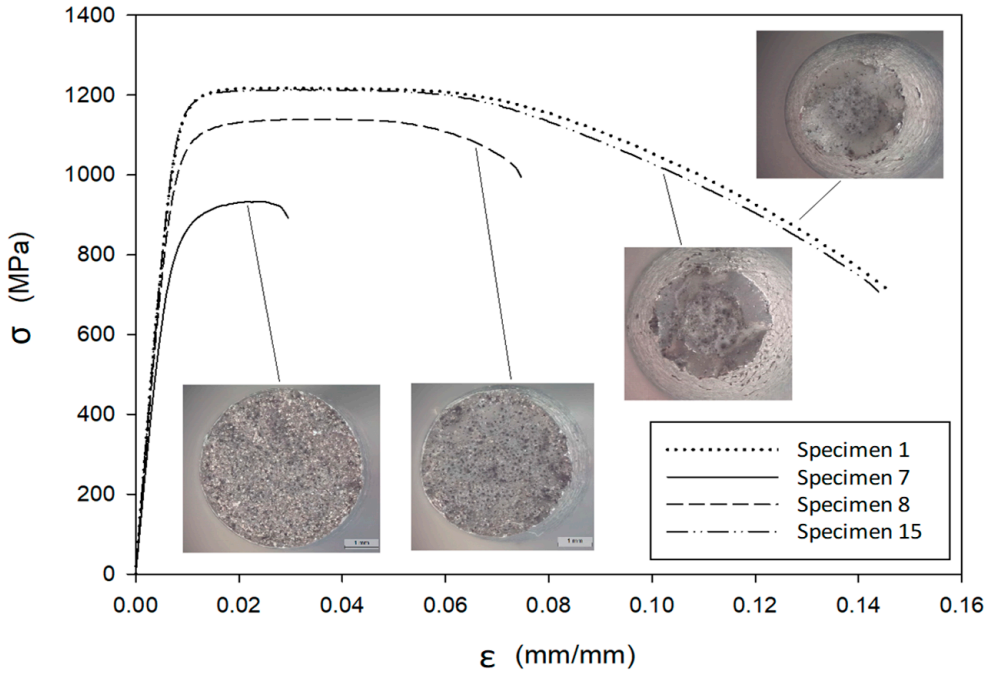

Figure 2. Stress–strain curves of the tested specimens.

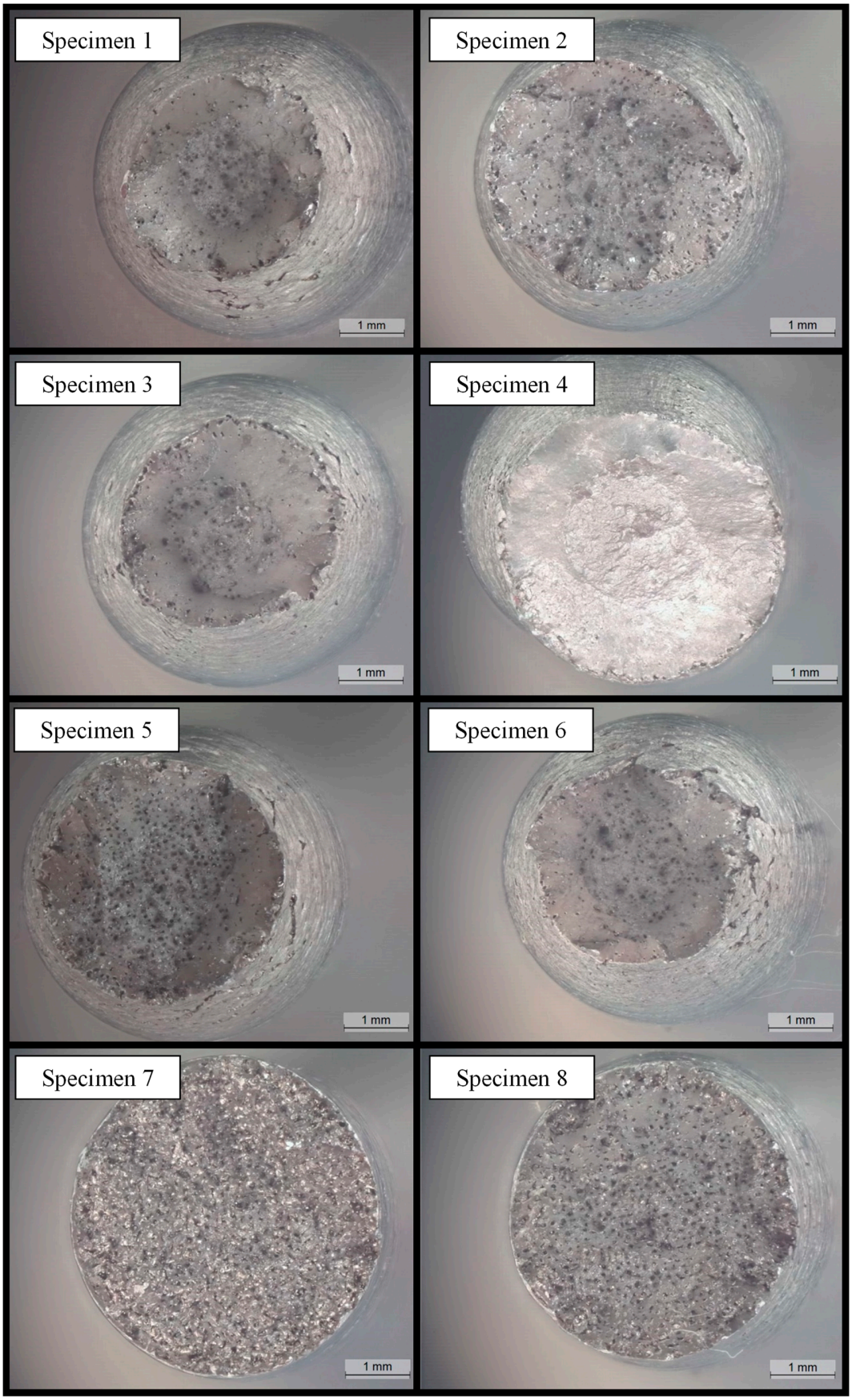

Figure 3. Optical micrographs of specimens 1 to 8.

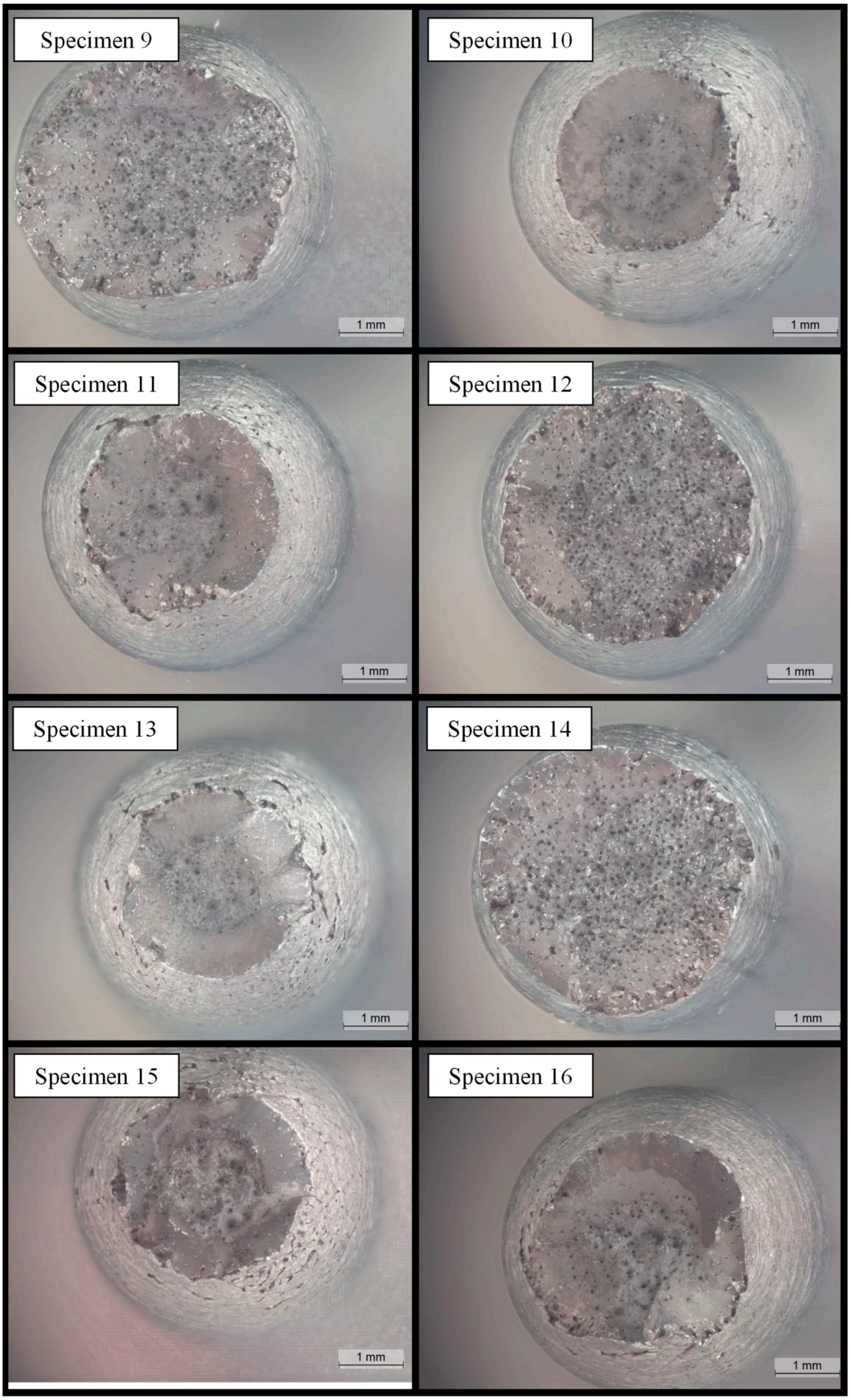

Figure 4. Optical micrographs of specimens 9 to 16.

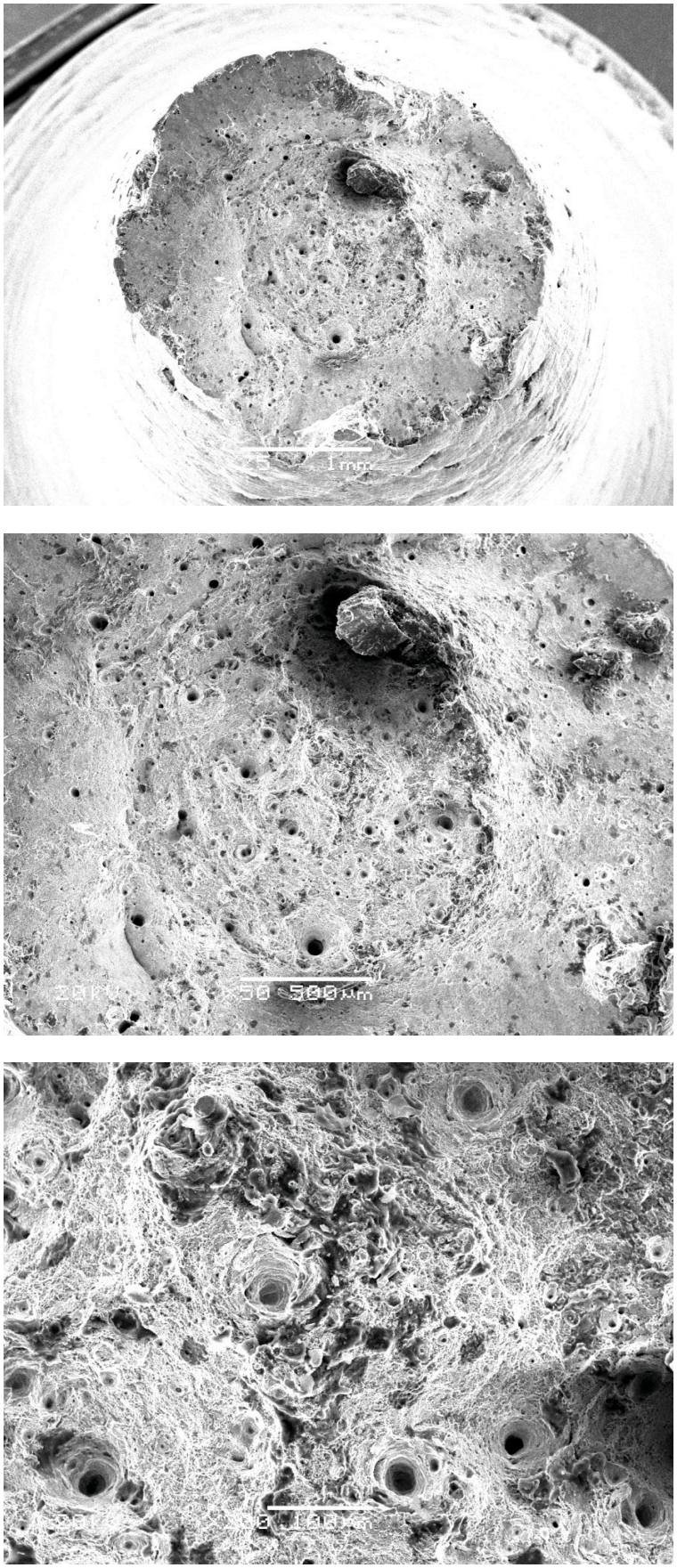

Figure 5. SEM micrographs (25×, 50× and 200×) of specimen 1.

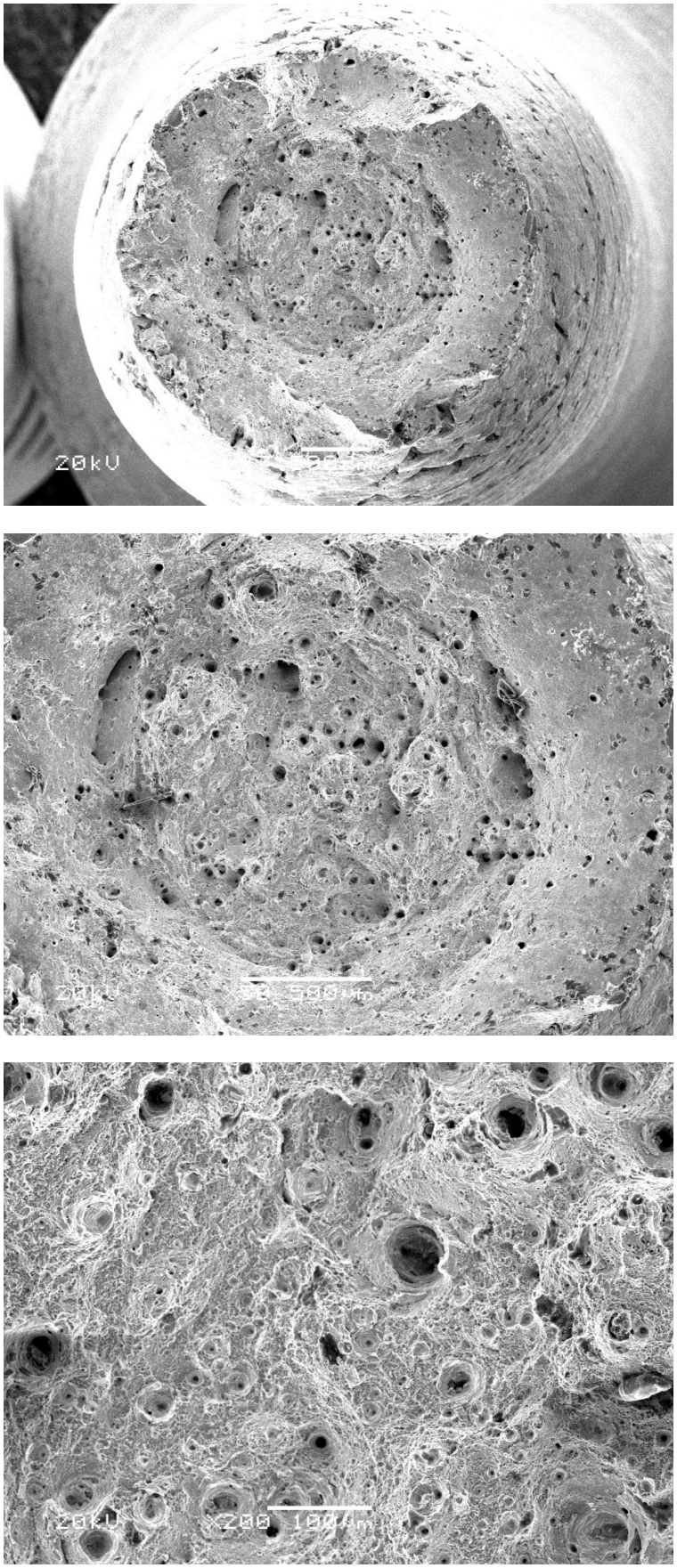

Figure 6. SEM micrographs (25×, 50× and 200×) of specimen 15.

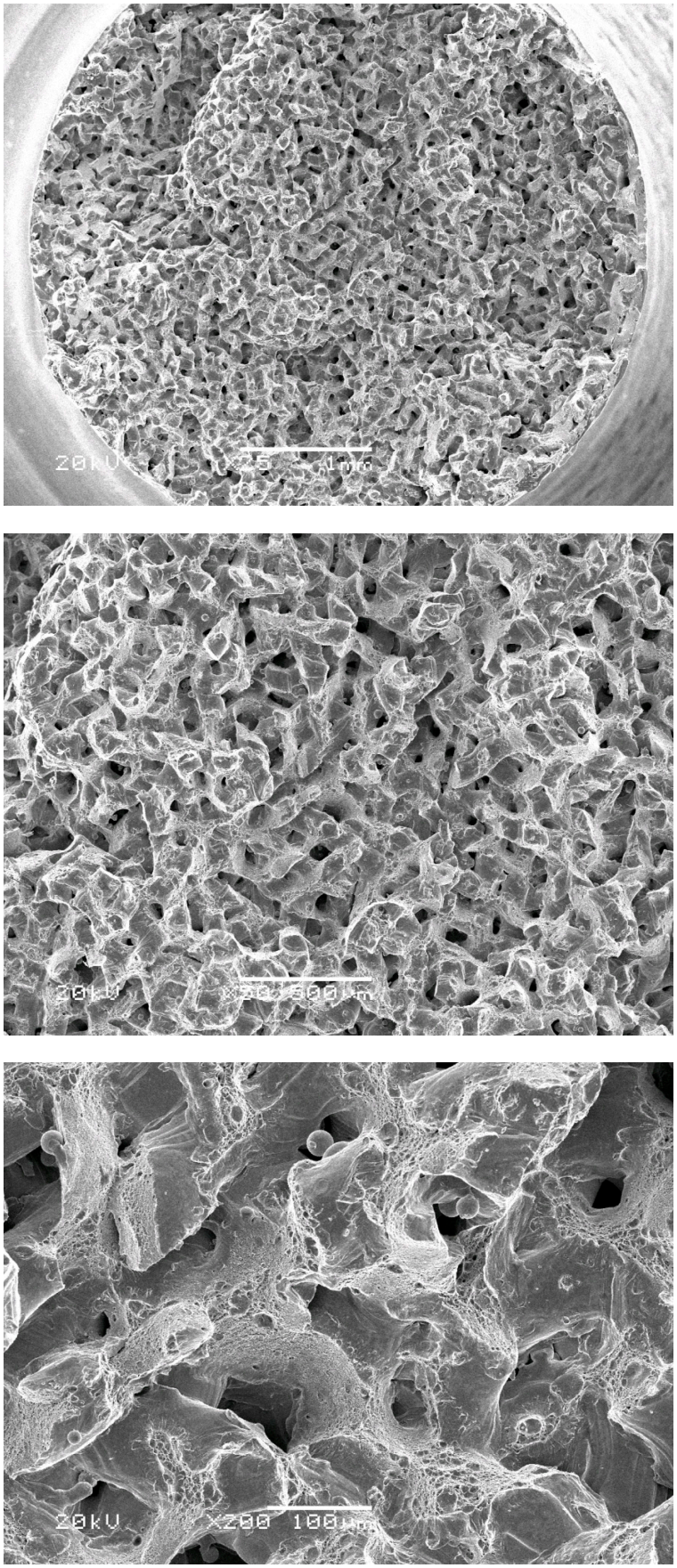

Figure 7. SEM micrographs (25×, 50× and 200×) of specimen 7.

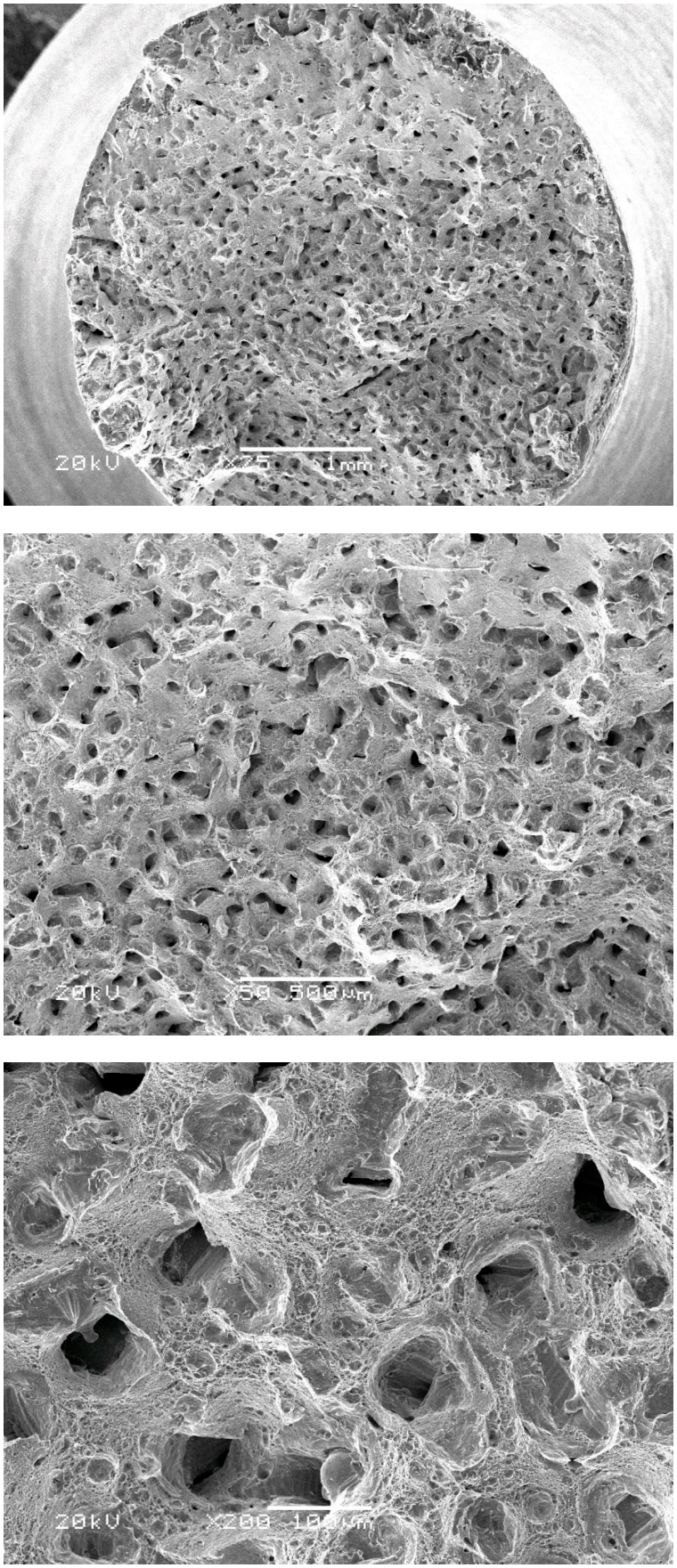

Figure 8. SEM micrographs (25×, 50× and 200×) of specimen 8.

For each of the stress–strain curves, the values of yield strength, ultimate stress, elongation and area under the curve have been obtained and can be found in Table 4. By introducing these values in the Design Expert software, it is possible to calculate the coefficients of the function $f(P^*, S^*, H^*)$ that defines the response surfaces of $\sigma_{0.2}$, σ_{uts}, ε_r and A, shown in expressions 3 to 6, respectively. The coefficients of determination (R^2) have been included for the corresponding fitted response surface.

$$f(P^*, S^*, H^*)_{\sigma_{0.2}} = 1144.93 + 25.81 \cdot P^* - 34.24 \cdot S^* - 45.70 \cdot H^* - 9.77 \cdot P^{*2} - \\ -31.92 \cdot S^{*2} - 17.52 \cdot H^{*2} + 26.37 \cdot P^* \cdot S^* + 39.85 \cdot P^* \cdot H^* - 56.87 \cdot S^* \cdot H^* \quad (3)$$
$$R^2 = 0.946$$

$$f(P^*, S^*, H^*)_{\sigma_{uts}} = 1258.44 + 26.72 \cdot P^* - 40.49 \cdot S^* - 47.28 \cdot H^* + 2.96 \cdot P^{*2} - \\ -29.81 \cdot S^{*2} - 14.63 \cdot H^{*2} + 18.63 \cdot P^* \cdot S^* + 40.90 \cdot P^* \cdot H^* - 40.74 \cdot S^* \cdot H^* \quad (4)$$
$$R^2 = 0.867$$

$$f(P^*, S^*, H^*)_{\varepsilon_r} = 12.53 + 1.08 \cdot P^* - 1.62 \cdot S^* - 2.75 \cdot H^* + 0.57 \cdot P^{*2} - \\ -1.65 \cdot S^{*2} - 1.16 \cdot H^{*2} + 0.39 \cdot P^* \cdot S^* + 1.10 \cdot P^* \cdot H^* - 1.46 \cdot S^* \cdot H^* \quad (5)$$
$$R^2 = 0.951$$

$$f(P^*, S^*, H^*)_A = 133.65 + 11.64 \cdot P^* - 18.37 \cdot S^* - 29.00 \cdot H^* + 7.86 \cdot P^{*2} - \\ -17.37 \cdot S^{*2} - 12.81 \cdot H^{*2} + 3.29 \cdot P^* \cdot S^* + 13.00 \cdot P^* \cdot H^* - 14.84 \cdot S^* \cdot H^* \quad (6)$$
$$R^2 = 0.948$$

Table 4. Values of the outcome variables of the experimental plan.

Test	$\sigma_{0.2}$ (MPa)	σ_{uts} (MPa)	ε_r (%)	*A* (MPa)
01	1145.7	1280.37	14.18	153.44
02	1089.5	1276.85	12.77	143.48
03	1162.2	1287.07	12.64	138.03
04	1160.1	1260.37	13.79	144.10
05	1096.1	1209.76	8.62	92.27
06	1147.9	1272.16	12.64	137.16
07	833.7	955.80	2.26	20.36
08	1042.4	1190.41	6.82	75.56
09	1111.3	1252.63	11.17	124.51
10	1167.2	1273.04	13.66	144.75
11	1147.9	1259.76	11.95	127.12
12	1086.3	1200.37	8.45	91.69
13	1141.3	1243.41	12.89	132.13
14	1121.7	1247.09	8.49	95.80
15	1151.3	1272.91	13.94	149.79
16	1122.2	1238.22	13.86	145.01

Figures 9–12 show the graphical representation of the response surfaces for all the analysed material properties ($\sigma_{0.2}$, σ_{uts}, ε_r and A) as a function of the coded variable parameters (P^*, S^* and H^*). Since the response surfaces depend on three input parameters, it is necessary to fix one of them for a 3D representation. To that purpose, the H^* value has been fixed with the three coded values (−1, 0 and 1). In the figures the solid dots represent the obtained experimental values.

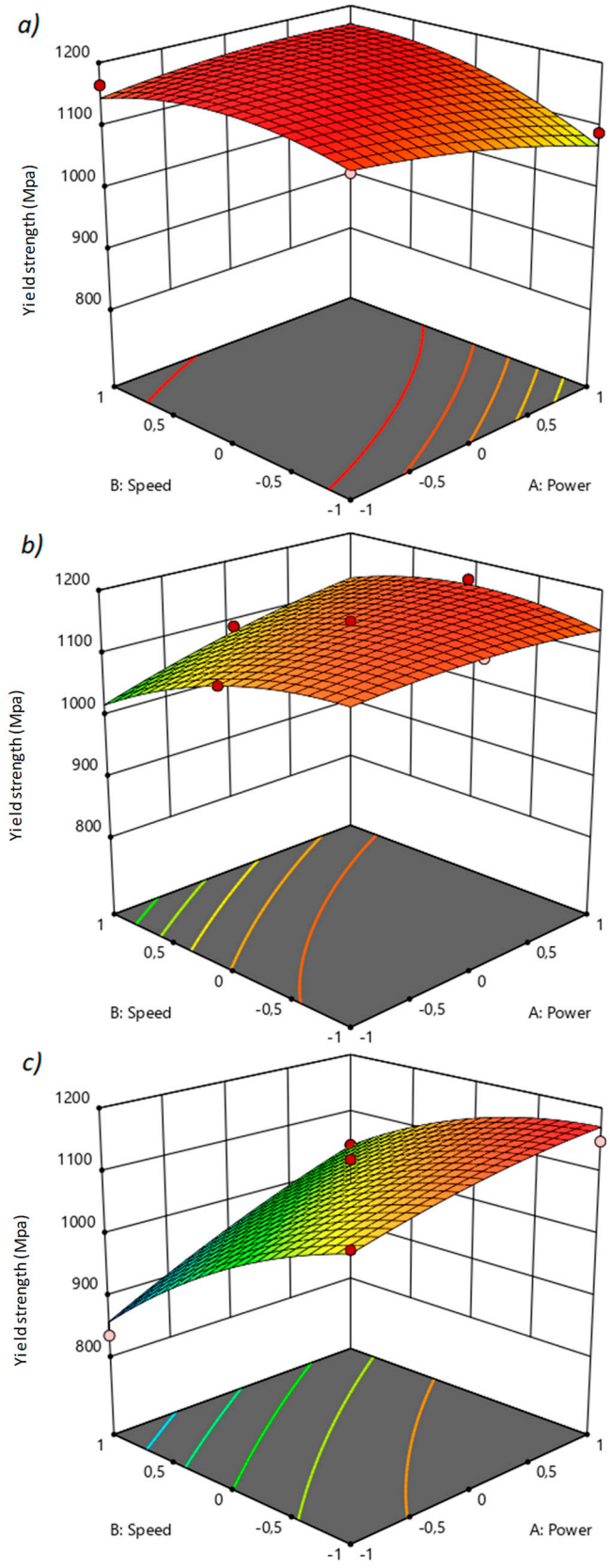

Figure 9. Response surfaces for $\sigma_{0.2}$, (**a**) $H^* = -1$ (**b**) $H^* = 0$ (**c**) $H^* = 1$.

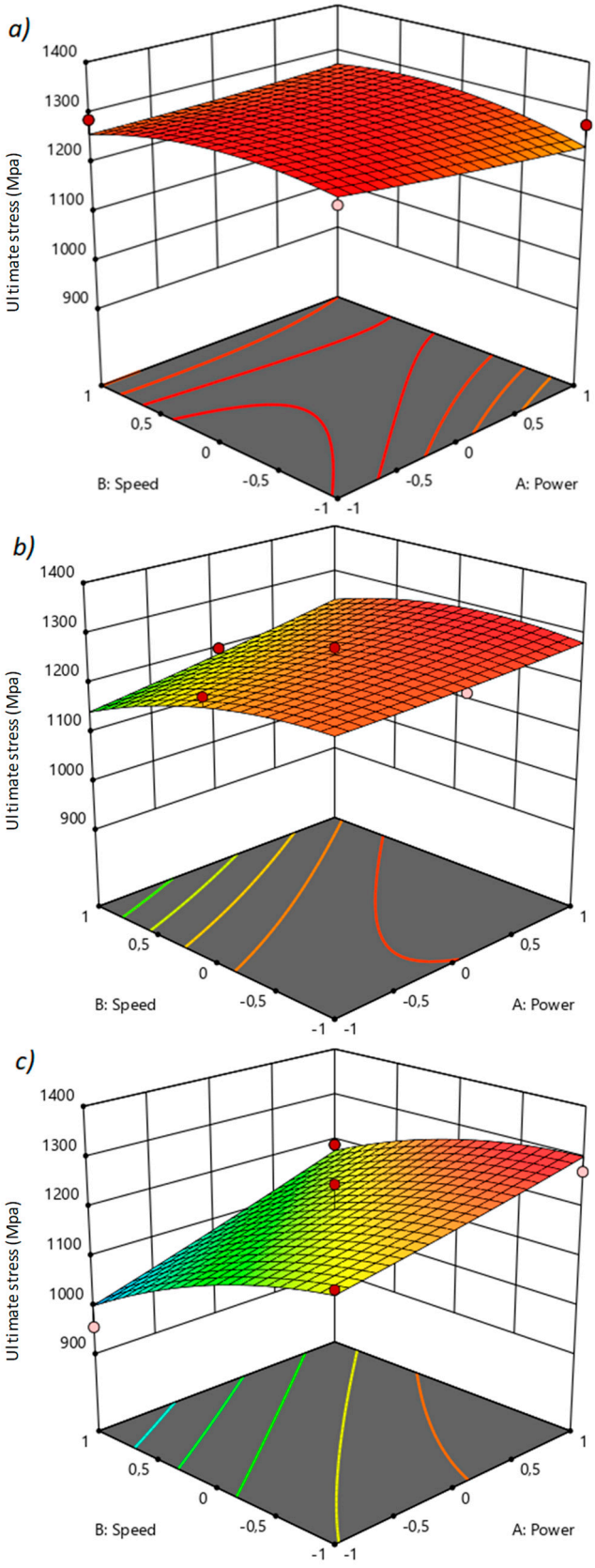

Figure 10. Response surfaces for σ_{uts}, (**a**) $H^* = -1$ (**b**) $H^* = 0$ (**c**) $H^* = 1$.

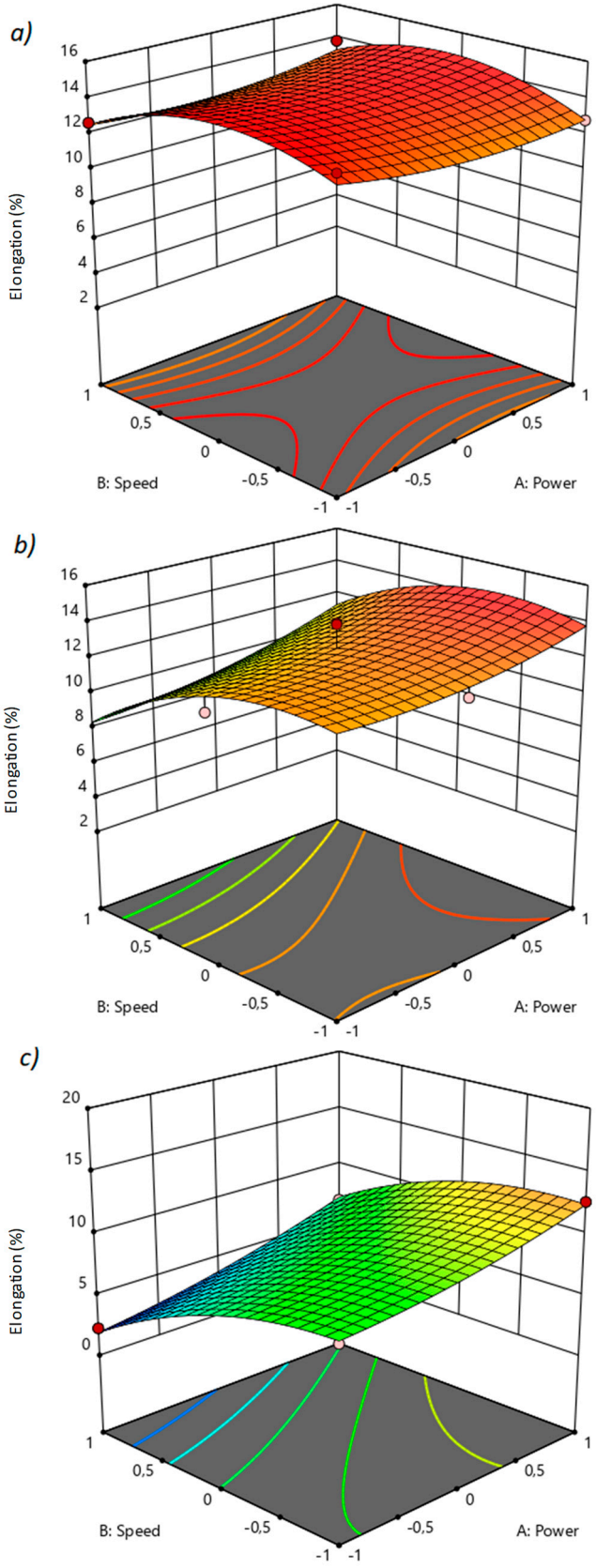

Figure 11. Response surfaces for ε_r, (**a**) $H^* = -1$ (**b**) $H^* = 0$ (**c**) $H^* = 1$.

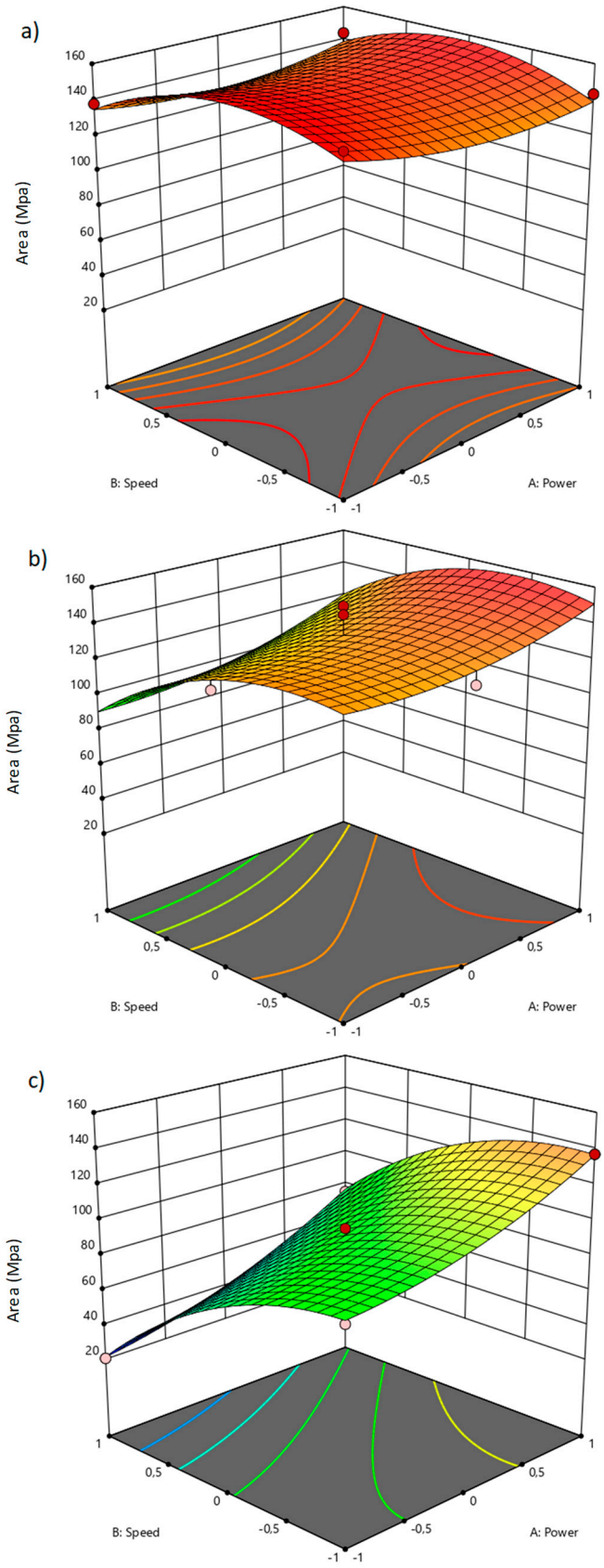

Figure 12. Response surfaces for A, (**a**) $H^* = -1$ (**b**) $H^* = 0$ (**c**) $H^* = 1$.

Once the above response surfaces have been fitted and represented, it is possible to obtain independently the maximum or minimum for each experimental outcome variable. However, in order to optimise the printing parameters (P, S and H), it is necessary that all of the mechanical properties are optimal, that is, that the values of $\sigma_{0.2}$, σ_{uts}, ε_r and A are maximised. This simultaneous maximisation would imply that the SLM C300 steel would have optimal mechanical properties. Consequently, the optimum combination has been considered as the point, within the established range, that maximises one or more responses. The nature of quadratic functions implies that they might have a critical point at which the partial derivatives are zero, but these points could be outside the domain of the experimental plan or be a minimum, which would invalidate them as feasible optimal combinations. To carry out this optimisation, a numerical algorithm in Matlab software has been used to localise the relative maximum point of each response surface within the experiment matrix. The procedure for finding the optimum point is based on the following steps:

1. Creation of a three-dimensional matrix n_3 with the values of P^*, S^* and H^*, within the range ([−1, 1], [−1, 1], [−1, 1]).
2. Calculation of the response to be optimised for each point by means of expressions 3 to 6 and the corresponding output matrix.
3. Obtaining the maximum response within the experiment matrix and its corresponding coded parameters $[P^*_{\max}, S^*_{\max}, H^*_{\max}]$.

Once the code has been implemented, the optimal parameters for each response are shown in Table 5. It can be seen that the optimal points do not agree between different responses and thus it is required to establish a tolerance value (tol) in order to identify an optimal value for the four responses simultaneously. In this sense, the valid points within the established tolerance value have been obtained from Expression (7). Figure 13 shows the clouds of valid points for each response for a tolerance of 1%. All of them have been grouped in Figure 14 where an optimum zone around the coded point [−1, −0.2, −1] can be observed for the point clouds. Therefore, this point corresponding to the printing parameters $P = 200\,W$, $S = 620\,mm/s$ and $H = 0.08\,mm$ can be considered as optimal for SLM fabrication of C300 steel.

Table 5. Optimal parameters for coded values $[P^*_{\max}, S^*_{\max}, H^*_{\max}]$.

$\sigma_{0.2}$	σ_{uts}	ε_r	A
[−0.54, 0.13, −1]	[−1, −0.31, −1]	[1, −0.08, −0.66]	[−1, −0.19, −1]

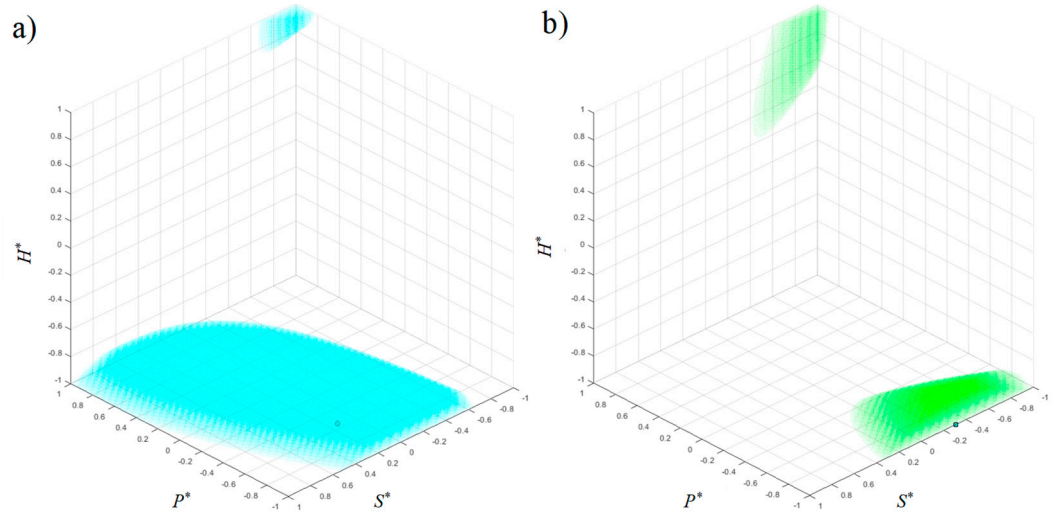

Figure 13. *Cont.*

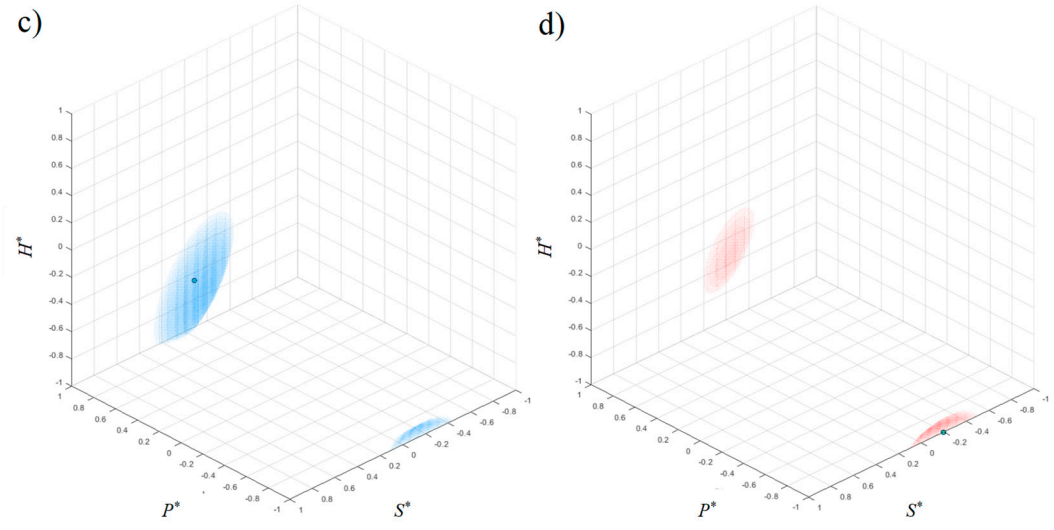

Figure 13. With a tolerance of 1% for (**a**) $\sigma_{0.2}$, (**b**) σ_{uts}, (**c**) ε_r and (**d**) A.

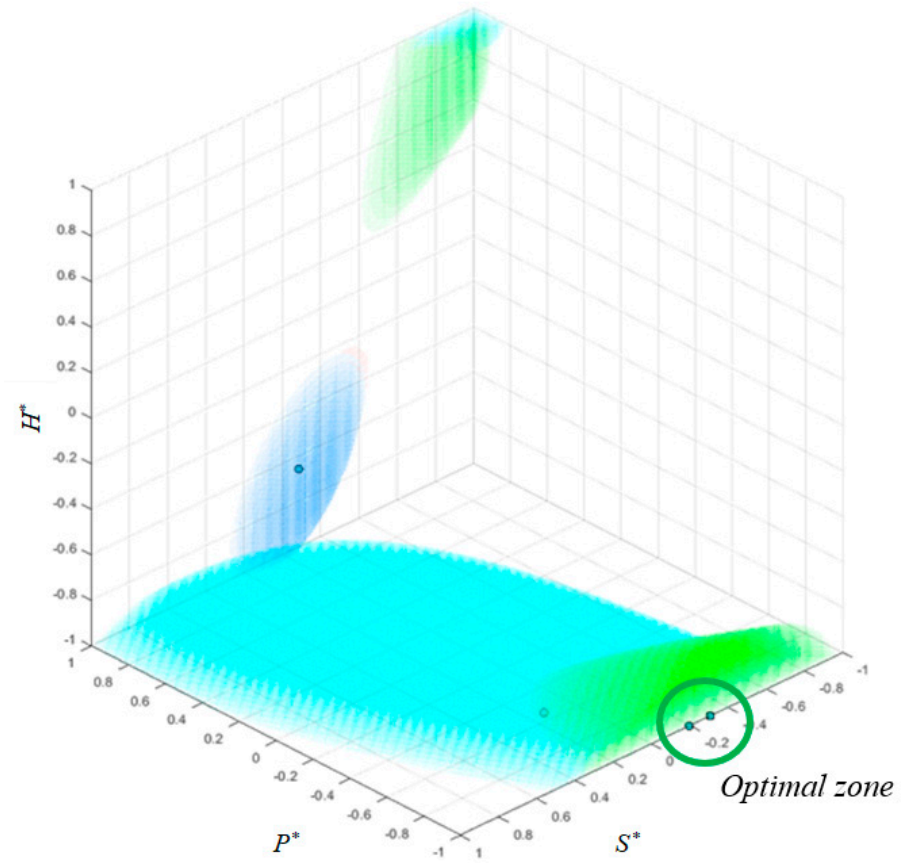

Figure 14. P^*_{val}, S^*_{val}, H^*_{val} grouped with a tolerance of 1%.

$$f(P^*_{val}, S^*_{val}, H^*_{val}) \geq \frac{(100 - tol)}{100} \cdot f(P^*_{\max}, S^*_{\max}, H^*_{\max}) \quad (7)$$

5. Conclusions

Response surfaces were obtained for the mechanical parameters analysed as experimental output variables ($\sigma_{0.2}$, σ_{uts}, ε_r and A) and the effect of the printing parameters (P, S and H) has been established. For the prediction of $\sigma_{0.2}$, σ_{uts}, ε_r and A for any combination of parameters P, S and H, the mathematical methodology employed in this paper can be

considered as a valid theoretical tool for this purpose. For this, it is necessary to establish a codification of the variable parameters and an appropriate experimentation plan.

Since each of the response surfaces had a different theoretical optimum point, it was necessary to set a tolerance of 1% around the optimum value to find a possible optimum zone. In this way, the following values: $P = 200\,\mathrm{W}$, $S = 620\,\mathrm{mm/s}$ and $H = 0.08\,\mathrm{mm}$ could be taken as possible optimal printing parameters. No doubt there will be other sets of parameter combinations for a suitable SLM production of C300 steel. In each case it will be up to the production engineers to decide which parameters to use.

The use of statistical methods, mechanical testing and data processing can be generalised and extended to other materials or range of parameters, so the process for determining the response surfaces would be analogous to the presented here.

Author Contributions: Conceptualization, I.I.C.; Funding acquisition, I.I.C. and J.M.A.; Investigation, I.I.C., A.D., M.A.R., L.B.P. and J.M.A.; Resources, J.M. All authors have read and agreed to the published version of the manuscript.

Funding: This research was funded by: INVESTUN/22/BU/0003 // BU-002-P20 // MU-21-UP2021-030.

Institutional Review Board Statement: Not applicable.

Informed Consent Statement: Not applicable.

Acknowledgments: The authors gratefully acknowledge financial support from the Junta de Castilla y Leon (Spain) through grants INVESTUN/22/BU/0003 and BU-002-P20, co-financed by FEDER funds. L.B. Peral is grateful for his Margarita Salas Postdoctoral contract (Ref.: MU-21-UP2021-030) funded by the University of Oviedo through the Next Generation European Union.

Conflicts of Interest: The authors declare no conflict of interest.

References

1. Günther, J.; Krewerth, D.; Lippmann, T.; Leuders, S.; Tröster, T.; Weidner, A.; Biermann, H.; Niendorf, T. Fatigue life of additively manufactured Ti–6Al–4V in the very high cycle fatigue regime. *Int. J. Fatigue* **2017**, *94*, 236–245. [CrossRef]
2. Shi, W.; Li, J.; Jing, Y.; Liu, Y.; Lin, Y.; Han, Y. Combination of Scanning Strategies and Optimization Experiments for Laser Beam Powder Bed Fusion of Ti-6Al-4V Titanium Alloys. *Appl. Sci.* **2022**, *12*, 6653. [CrossRef]
3. Kruth, J.-P.; Mercelis, P.; Van Vaerenbergh, J.; Froyen, L.; Rombouts, M. Binding mechanisms in selective laser sintering and selective laser melting. *Rapid Prototyp. J.* **2005**, *11*, 26–36. [CrossRef]
4. Hind, A.; Maalouf, M.; Barsoum, I.; An, H. Truncated Newton Kernel Ridge Regression for Prediction of Porosity in Additive Manufactured SS316L. *Appl. Sci.* **2022**, *12*, 4252. [CrossRef]
5. Leary, M. Surface roughness optimisation for selective laser melting (SLM): Accommodating relevant and irrelevant surfaces. In *Laser Additive Manufacturing*; Woodhead Publishing: Thorston, UK, 2017; pp. 99–118.
6. Yang, K.-R.; Hanawa, T.; Kwon, T.-Y.; Min, B.-K.; Hong, M.-H. Mechanical Property Comparison of Ni–Cr–Mo Alloys Fabricated via One Conventional and Two New Digital Manufacturing Techniques. *Appl. Sci.* **2021**, *11*, 9308. [CrossRef]
7. Kasperovich, G.; Hausmann, J. Improvement of fatigue resistance and ductility of TiAl6V4 processed by selective laser melting. *J. Mater. Process. Technol.* **2015**, *220*, 202–214. [CrossRef]
8. Hudák, R.; Schnitzer, M.; Králová, Z.; Gorejová, R.; Mitrík, L.; Rajťúková, V.; Tóth, T.; Kovačević, M.; Riznič, M.; Oriňaková, R.; et al. Additive Manufacturing of Porous Ti6Al4V Alloy: Geometry Analysis and Mechanical Properties Testing. *Appl. Sci.* **2021**, *11*, 2611. [CrossRef]
9. Courtright, Z.S.; Leclerc, N.P.; Kim, H.N.; Kalidindi, S.R. Critical Comparison of Spherical Microindentation, Small Punch Test, and Uniaxial Tensile Testing for Selective Laser Melted Inconel 718. *Appl. Sci.* **2021**, *11*, 1061. [CrossRef]
10. Yap, C.Y.; Chua, C.K.; Dong, Z.L.; Liu, Z.H.; Zhang, D.Q.; Loh, L.E.; Sing, S.L. Review of selective laser melting: Materials and applications. *Appl. Phys. Rev.* **2015**, *2*, 041101. [CrossRef]
11. Zhang, B.; Li, Y.; Bai, Q. Defect Formation Mechanisms in Selective Laser Melting: A review. *Chin. J. Mech. Eng.* **2017**, *30*, 515–527. [CrossRef]
12. Naceur, H.; Ben-Elechi, S.; Batoz, J.; Knopf-Lenoir, C. Response surface methodology for the rapid design of aluminum sheet metal forming parameters. *Mater. Des.* **2007**, *29*, 781–790. [CrossRef]
13. Dehghani, K.; Nekahi, A.; Mirzaie, M.A.M. Using response surface methodology to optimize the strain aging response of AA5052. *Mater. Sci. Eng. A* **2010**, *527*, 7442–7451. [CrossRef]
14. Cuesta, I.; Alegre, J.M. Determination of plastic collapse load of pre-cracked Small Punch Test specimens by means of response surfaces. *Eng. Fail. Anal.* **2012**, *23*, 1–9. [CrossRef]

15. Wei, L.; Yuying, Y.; Zhongwen, X.; Lihong, Z. Springback control of sheet metal forming based on the response-surface method and multi-objective genetic algorithm. *Mater. Sci. Eng. A* **2009**, *499*, 325–328. [CrossRef]
16. Hoseini, S.R.E.; Arabi, H.; Razavizadeh, H. Improvement in mechanical properties of C300 maraging steel by application of VAR process. *Vacuum* **2008**, *82*, 521–528. [CrossRef]
17. Dehgahi, S.; Sanjari, M.; Ghoncheh, M.; Amirkhiz, B.S.; Mohammadi, M. Concurrent improvement of strength and ductility in heat-treated C300 maraging steels produced by laser powder bed fusion technique. *Addit. Manuf.* **2021**, *39*, 101847. [CrossRef]
18. Khuri, A.I.; Cornell, J.A. *Response Surfaces. Design and Analyses, Statistics: Textbooks and Monographs*; Marcel Dekker: New York, NY, USA, 1987; p. 81.
19. Kuehl, R.O. *Diseño de Experimentos*; International Thomson: St Miami, FL, USA, 2001.
20. Montgomery, D.C. *Diseño y Análisis de Experimentos*; Grupo Editorial Iberoamérica: Mexico City, Mexico, 1991.
21. *ASTM E8/E8M-16a*; Standard Test Methods for Fire Tests of Building Construction and Materials. ASTM International: West Conshohocken, PA, USA, 2018. Available online: https://www.astm.org/ (accessed on 1 June 2022).